Thermal Performance Analysis of a Scaled-up Suspension Flow Receiver for Generation of Industrial Process Heat: A Computational Study

Daniel Ang[1, a)], Yining Tang[1], Alfonso Chinnici[1], Zhao F. Tian[1], Woei L. Saw[2], Timothy Lau[3], Philip Ingenhoven[2], Zhiwei Sun[1], and Graham J. Nathan[1]

[1]*School of Mechanical Engineering, Centre for Energy Technology, The University of Adelaide, SA 5005, Australia*
[2]*School of Chemical Engineering and Advanced Materials, Centre for Energy Technology, The University of Adelaide, SA 5005, Australia*
[3]*UniSA STEM, University of South Australia, Mawson Lakes, SA 5095, Australia*

[a)] Corresponding author: danieljintung.ang@adelaide.edu.au

Abstract. Emerging directly irradiated particle receiver technologies have the capability of generating temperatures exceeding 800ºC. This is important for industrial processes involving high temperatures, such as electricity generation and thermochemical processes, such as the Bayer alumina process. The utilization of particles in these devices is receiving growing attention due to their potential to withstand high temperatures and their effectiveness on solar radiation absorption. Among all particle receiver technologies being developed globally, the suspension flow receiver, better known as a vortex flow receiver, is receiving growing attention as a method to heat particles in suspension, and hence to heat both phases. In this study, a set of novel scale-up strategies was investigated for a 50-MW windowless directly irradiated vortex-based solar particle receiver to identify the strengths and limitations of each strategy. A receiver design was determined and chosen as the candidate for the current computational study. A systematic analysis was performed to assess the influence of particle mass loading and inlet air mass flowrate on the global performance of the receiver at scale (50-MW) under steady-state conditions with simulated solar flux, along with CARBO-CP used as the particle material. A fixed ratio of overventilation was applied to the induced draft fan to reduce particle egress. The numerical study was conducted using computational fluid dynamics (CFD) software (ANSYS/CFX 2020 R2). The result predicts that up to 60% thermal efficiency can be achieved under high air mass flowrates and particle loadings at scale for the operating conditions analyzed here.

INTRODUCTION

Global CO_2 emissions from heavy industry account for about 15% of the anthropogenic sources, which can be difficult to abate as high temperatures are needed to produce products such as steel, aluminium, and cement (1-3). The implementation of concentrated solar thermal energy technologies (CST) can potentially contribute to meeting this challenge, particularly via one or more of several particle-based solar receiver technologies, which can achieve temperatures exceeding 700ºC (4). The utilization of solid particles in concentrated solar thermal systems has the potential to be beneficial due to its ability to withstand high temperatures and its efficient absorption of radiant energy. Of the various classes of particle flow technologies, the solar expanding vortex receiver (SEVR) has particular advantages and disadvantages. Its operation with particles in suspension achieves a relatively long exposure time of particles to the concentrated solar radiation, offering a highly efficient way to heat both phases (5). The heating of both phases makes it well suited to the heating of reacting flow but also requires a method to recover heat from the second phase if it is being used to heat only one of the two phases. The current receiver configuration constitutes a further development of the original vortex receiver proposed by ETH/PSI, through a windowless configuration,

seeking to avoid the operational and maintenance costs, including preventing the risk of window failure (6, 7). Nevertheless, this requires the development of a suitable configuration to mitigate convective heat losses.

The objective of the present investigation is to estimate the potential performance of the SEVR for the application to supplying industrial process heat with a target operating temperature with ranges between 950ºC – 1100ºC at a scale of 50 MW solar thermal input from the heliostat field. This temperature is relevant to processes such as steam methane reforming as well as calcination of gibbsite or lime indirectly (8, 9). This differs from previous works on the SEVR, which has been performed at the laboratory scale, resulting in a lack of thermal performance data for the scaled-up device. Despite numerical modelling has been applied to previous studies, there is a need to test the confidence of the CFD tool at scale. In addition, there is also a lack of understanding of the scale-up criteria for a solar particle receiver of this class. Therefore, the present paper aims to meet the need through CFD simulation.

METHODOLOGY

Scaling up a Solar Receiver

Several scaling criteria have been proposed for scaling up lab-scale burners/furnaces, cyclones and calciners (10-12). These can be assessed for the upscaling of a suspended flow solar receiver. The three standard scaling criteria used for such devices can be categorized into three methods: constant velocity (CV), constant residence time (CRT), and the Hybrid approach.

The CV approach maintains the inlet velocity to the receiver to be constant at different scales, while the dimensions are derived based on Equation 1. In contrast, the CRT approach assumes that the nominal residence time of the receiver ($\tau = V/Q$) is held constant, with the physical dimensions determined through the relationship as shown in Equation 2. The hybrid approach, also known as Cole's approach, assumes that both inlet velocity and inlet jet area are increased equally with the receiver, with the geometrical dimensions defined by Equations 3&4. Here, D represents the jet diameter at the inlet. At the same time, P is the total fixed input solar power into the receiver.

$$\textbf{CV}: \frac{D_{jet,scale-up}}{D_{jet,lab-scale}} = \sqrt{\frac{P_{scale-up}}{P_{lab-scale}}}, \tag{1}$$

$$\textbf{CRT}: \frac{D_{jet,scale-up}}{D_{jet,lab-scale}} = \sqrt[3]{\frac{P_{scale-up}}{P_{lab-scale}}}, \tag{2}$$

$$\textbf{Hybrid}: \frac{U_{jet,scale-up}}{U_{jet,lab-scale}} = \sqrt{\frac{P_{scale-up}}{P_{lab-scale}}}, \tag{3}$$

$$\frac{D_{jet,scale-up}}{D_{jet,lab-scale}} = \sqrt[4]{\frac{P_{scale-up}}{P_{lab-scale}}}, \tag{4}$$

A logic diagram has been created to assist with scaling up the solar receiver, as shown in Figure 1. The receiver length-to-cavity diameter (L/D_c) ratio was fixed at 1.25. It was previously reported that this ratio matches the design criteria as the reference case for the lab-scale receiver for the aerodynamics and heat transfer within the receiver (5, 13). The process begins by determining the aerodynamic criteria through hand calculations with Equations 1 – 4. By assessing all three criteria, the design criteria with the impractical jet diameter/velocity are eliminated. Once the suitable criteria have been identified, the number of inlets and outlets required for the device is calculated with the assumptions provided. The appropriate number of inlet/outlet jets is evaluated by determining the Reynolds (Re) and Stokes (Sk) numbers at the inlet. This is to ensure that the particle-laden flow is fully turbulent to generate a swirling flow, as well as particle trajectory follows the fluid stream. Once the constraints are met, the geometry of the receiver is designed through the calculation of the aperture size and cavity diameter under a fixed total input of solar flux on the aperture. The geometry is defined, and the most compact receiver design is selected from the remaining strategies. With the specified criteria, the scaled-up receiver geometry is created for CFD simulations. Once the simulation results have been obtained, the thermal efficiency and temperature trend are compared to ensure that the result correlates well

with the lab-scale device. The process is iterated until a geometry is determined. After the geometry has been determined, a preliminary systematic study is conducted to understand the thermal performance of the receiver at scale.

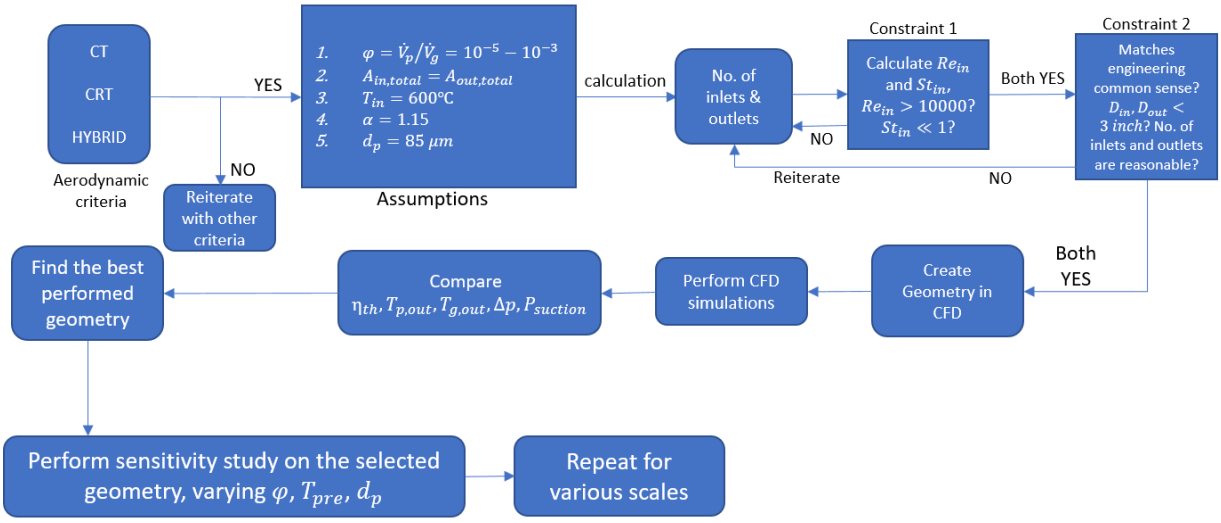

FIGURE 1. Logic diagram for the scaling-up procedure of the SEVR.

Numerical Model and Operating Conditions

The schematic diagram of a scaled-up 50 MW windowless SEVR used for this numerical study is shown in Figure 2a. For this particular study, the geometrical parameters and operational conditions of the receiver are presented in Tables 1 & 2. It is worth noting that an active aerodynamic strategy through a fixed overventilation ($\alpha = 100\left[\frac{\dot{m}_{a,o} - \dot{m}_{a,i}}{\dot{m}_{a,i}}\right]$) was applied at the outlet to mitigate the particle egress from the receiver aperture (14). Both single and two-phase tests were conducted to systematically assess the coupled influence of fluid flowrate and particle loading on the global thermal performance (i.e., thermal efficiency, outlet temperature and particle egress) of the receiver. The Monte Carlo ray-tracing approach was employed for the radiation model. In the numerical model, the Gaussian distribution solar flux input (50MW) is modelled using the expression function adopted based on the study of Steinfeld and Schubnell, as shown in Figure 2b (15). This was applied due to the absence of reliable data from the high flux field at 50MW.

TABLE 1. Geometrical parameters of the scaled-up 50 MW SEVR.

Geometrical Parameters	50MW-SEVR
D_c, Cylinder diameter [mm]	7750
D_{in}, Inlet diameter [mm]	500
L_c, Cylinder length [m]	8540
D_b, Base diameter [mm]	1940
θ, Cone angle [°]	50
D_{ap}, Aperture diameter [mm]	3900
D_{out}, outlet diameter [mm]	1590
L, total length [mm]	12500
no. of inlets	12
no. of outlets	12

TABLE 2. Proposed operating parameters for the scaled-up 50 MW SEVR.

Operational Conditions	50MW-SEVR
$\dot{m}_{a,i}$, Inlet air mass flowrate [kg/s]	24, 42
$\dot{m}_{p,i}/\dot{m}_{a,i}$, Particle mass loading	0.05 – 1.3
T_{in}, Inlet air and particle temperature [°C]	600
α, overventilation [%]	15

The geometry of the 50MW SEVR was constructed in Design Modeler with details provided in Table 1, along with unstructured mesh generated using ANSYS/Meshing 2020 R2. The mesh independence test is conducted with three mesh sizes (0.4, 0.85, 1.5 million nodes). Shear-stress-transport (SST) turbulence model with turbulent dispersion is applied as a good agreement is found in the flow field of previous studies involving swirling flows (16). In each simulation, 50,000 fully spherical CARBO-CP ceramic particles with a mean particle size of 85 microns are injected into the receiver. The setting of the Lagrangian model is applied to track the trajectory of each particle in the computational domain. The SIMPLE algorithm was employed, while all equations were discretized using the second-order upwind scheme.

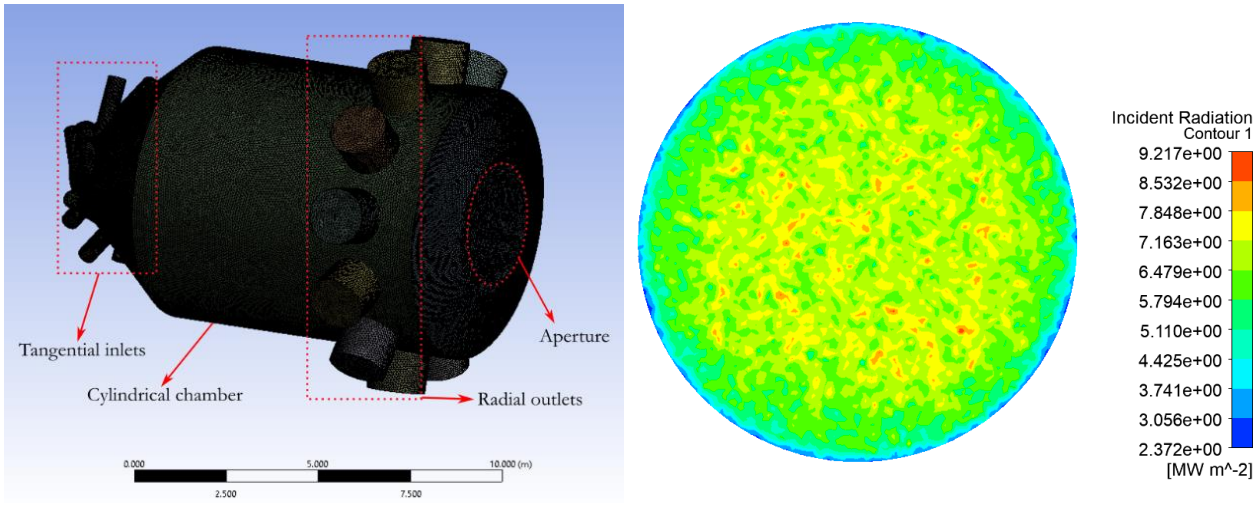

(a) (b)

FIGURE 2. (a) Schematic diagram of the scaled-up 50 MW SEVR CFD model. (b) Radiation flux profile at the aperture plane.

Thermal Performance Analysis

The overall thermal efficiency of the receiver is based on the energy balance equation, which can be described as follows:

$$\eta_{th} = 100\left[\frac{\dot{m}_{a,o}\, c_{p,a}(T_{a,o}-T_{a,i}) + \dot{m}_{p,o}\, c_{p,p}(T_{p,o}-T_{p,i})}{\dot{Q}_{total}}\right], \quad (5)$$

Here, $\dot{Q}_{total}$ is the total solar thermal flux input into the system, where, $c_{p,a}$ and $c_{p,p}$ are specific heat capacity of gas and particles, $T_{a,o}$ and $T_{p,o}$ are outlet temperatures of gas and particles at the outlet, while $\dot{m}_{a,o}$ and $\dot{m}_{p,o}$ is the total mass flowrate of air and particles at the outlet. For the current calculation, it is assumed that no particles are lost in the process (i.e., $\dot{m}_{p,i} = \dot{m}_{p,o}$) with an excess overventilation (α) (i.e., 15%) of air applied at the outlet to mitigate particle egress through the aperture.

RESULTS AND DISCUSSION

Table 3 presents the results obtained from the three different scale-up strategies, CV, CRT, and hybrid. It can be seen that, for the hybrid approach, the inlet velocity exceeds the operational velocity range of 20 – 45 m/s. Hence, this option can be directly eliminated from the scale-up criteria. As for the CV approach, it can be seen that the inlet velocity and the number of inlet ports falls in a reasonable range in meeting the design criteria. However, one of the trade-offs from this approach is that the receiver size is larger, which increases the capital cost of the technology.

Furthermore, the longer residence time of the receiver is not feasible for applications in calcination or particle heating, where the feedstock usually dwells within the device for an order of seconds (8). As seen in the table, the CRT approach was favoured as the residence time and inlet velocity meets the requirement found in thermochemical process reactors (11). It can also be seen that this strategy can achieve the most compact geometrical design compared to others. Therefore, the constant residence time (CRT) approach is chosen as the design strategy for the current solar receiver.

TABLE 3. Results from the scale-up criteria.

Parameters	CV	CRT	Hybrid
Inlet Velocity [m/s]	30	42	300
Residence Time [s]	115	5	N.C[1]
Number of Inlets	6	12	N.C
Aperture diameter [m]	10	5.8	N.C
Receiver Length [m]	33	18	N.C

Figure 3a presents the mean air, $T_{a,o}$, and particle, $T_{p,o}$, outlet temperature of the 50MW SEVR for a fixed overventilation as a function of particle mass loading ($\dot{m}_{p,i}/\dot{m}_{a,i}$). From the figure, the temperature decreases with the inlet air mass flowrate. The increment of flowrate results in temperature drops due to temperature rise through energy balance, similar to that found in Chinnici et al., (14). Consequently, the temperature of air increases logarithmically with the increment of particle loading. This shows that particles act as an enhancer in absorbing radiant energy to boost temperature within the device.

Figure 3b presents the overall thermal efficiency, $\eta_{th,overall}$, with the variation of the inlet mass flowrate, $\dot{m}_{a,i}$. The trend of flowrate was expected as the temperature rise was reduced. In addition, the overall is higher when particles are added into the system. This is expected as the addition of particles increases the amount of heat absorbed

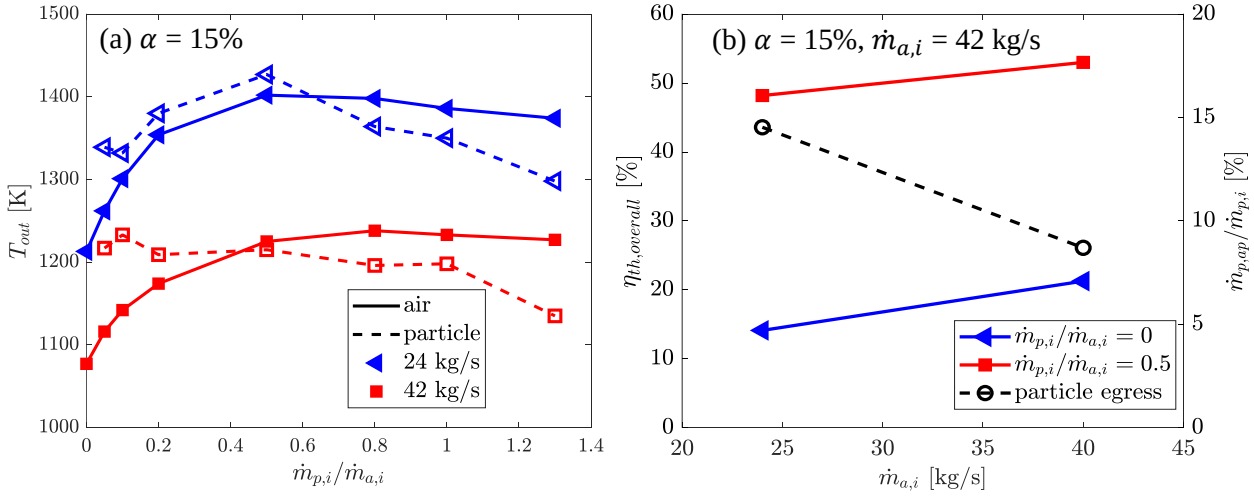

FIGURE 3. Calculated values of (a) Mean outlet temperature of the air ($T_{a,o}$) and particle phase ($T_{p,o}$) of the receiver as a function of particle mass loading ($\dot{m}_{p,i}/\dot{m}_{a,i}$). (b) Thermal efficiency, $\eta_{th,overall}$, and particle egress ($\dot{m}_{p,ap}/\dot{m}_{p,i}$) at fixed particle loading of 0.5, as a function of inlet air mass flowrate ($\dot{m}_{a,i}$).

[1] N.C: Not Calculated.

by the flow. The increment of flowrate also shows that particle egress ($\dot{m}_{p,ap}/\dot{m}_{p,i}$) is reduced from 13% to 8% at a fixed particle loading of 0.5, mainly due to the higher tangential velocity generated by swirling flow, allowing particles to be centrifuged more closely to the reactor wall while reducing the number of particles being recirculated through the aperture as was reported (17).

Figure 4 presents the calculated thermal efficiency as a function of particle mass loading, $\dot{m}_{p,i}/\dot{m}_{a,i}$, for the two-phase flow, $\eta_{th,overall}$, along with the separate air and particle phases ($\eta_{th,air}, \eta_{th,particle}$). Data are reported for two values of inlet mass flowrate, $\dot{m}_{a,i}$. As shown in Figure 4a, the overall thermal efficiency increases as the loading increases. This is because, as reported in Figure 3a, the increment of loading leads to increased absorption of radiant energy by particles.

Similarly, Figure 4b reports that the thermal efficiency of the gas-phase increases logarithmically as loading increases. This correlates well with the particle phase, as convective heat loss is transferred from the particles to the air, thereby enhancing the temperature of the air.

Figure 4c presents the thermal efficiency of the particle phase. Similarly, an increase in particle loading causes an increase in thermal efficiency due to the increased energy absorbed. It is important to note that the absorption of radiant heat from the solar input involves a non-linear and complex relationship. Hence, the curve trend increases linearly at a lower loading while the slope gradient reduces upon reaching a higher loading.

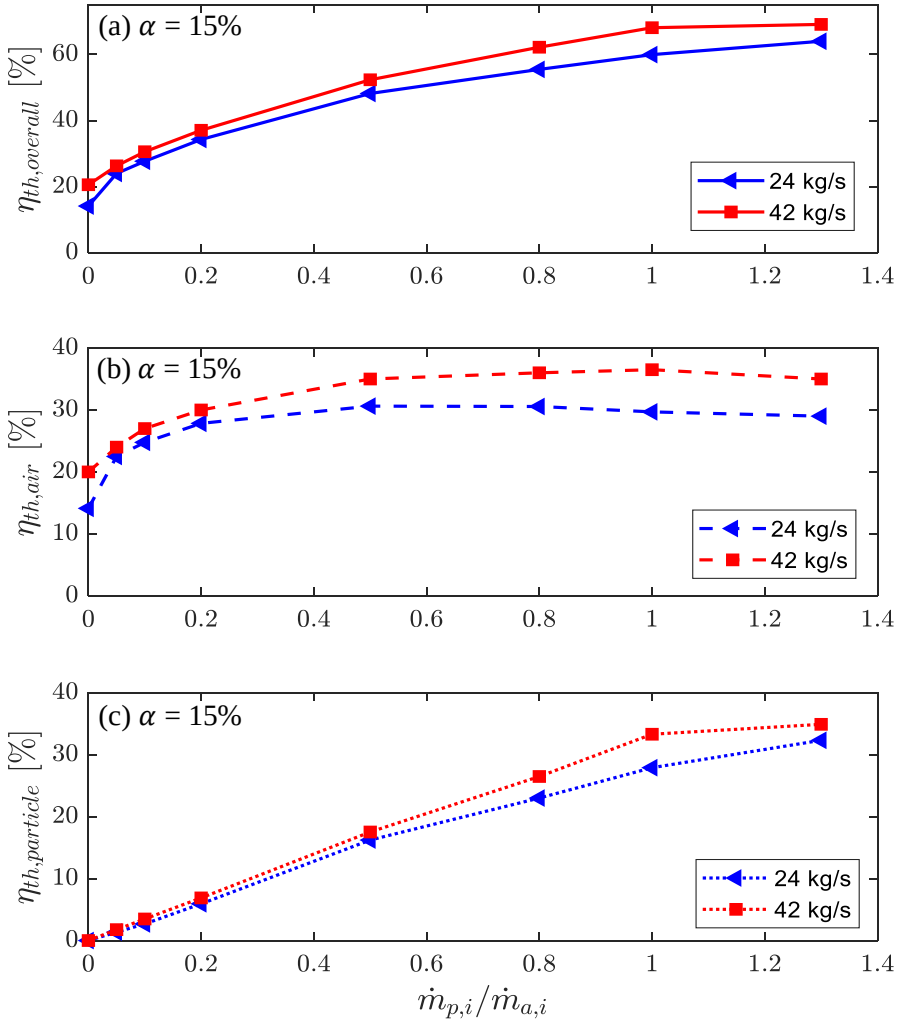

FIGURE 4. Thermal efficiency of the (a) two-phases, $\eta_{th,overall}$, (b) gas phase, $\eta_{th,air}$, (c) particle phase, $\eta_{th,particle}$, as a function of particle mass loading ($\dot{m}_{p,i}/\dot{m}_{a,i}$).

CONCLUSION

The key outcomes of the numerical investigation on the scaled-up windowless vortex-based particle receiver are as follows:

- The theoretical calculations from the scale-up criteria of the SEVR show that the constant particle residence time approach is the most suitable. This is because it features the most compact design for the device. For the application of a central tower top configuration, the compact size of the reactor is feasible as it reduces operational, maintenance and any other additional on-costs.

- The sensitivity study on the thermal performance of the SEVR to the particle and air mass flowrate shows that the inlet air mass flowrate has a controlling influence on the performance of the SEVR. The addition of particles has proven effective in enhancing the thermal efficiency of the reactor, which is due to the increased radiative heat absorption to the surface area of the particles from the solar input. For the operating conditions analyzed here, the thermal efficiency of the receiver is estimated at around 60% under high air mass flowrate and particle loading. The particle egress rate was found to be approximately 8% under a high mass flowrate with a fixed particle mass loading of 0.5.

- Particle egress was found to reduce as the inlet flow velocity is increased. This is attributed to increased centrifugal forces, moving the particles closer to the receiver wall and further away from the aperture, thereby, reducing the number of particles recirculated through the aperture. It is also accompanied by an increase in efficiency, which is probably linked to this reduction in egress.

ACKNOWLEDGEMENT

The authors gratefully acknowledge the support of the Australian Renewable Energy Agency, ARENA, through the RND054 Bayer program.

REFERENCES

1. Pedraza J, Zimmermann A, Tobon J, Schomäcker R, Rojas N. On the road to net zero-emission cement: Integrated assessment of mineral carbonation of cement kiln dust. Chemical Engineering Journal. 2021;408:127346.
2. Wang P, Ryberg M, Yang Y, Feng K, Kara S, Hauschild M, et al. Efficiency stagnation in global steel production urges joint supply- and demand-side mitigation efforts. Nature Communications. 2021;12(1):2066.
3. Saw WL, Naufal A, Sandoval AB, Beath A, Lovegrove K, van Eyk P, et al., editors. Technical feasibility of integrating concentrating solar thermal energy in the Bayer alumina process. AIP Conference Proceedings; 2020: AIP Publishing LLC.
4. Ho CK. A review of high-temperature particle receivers for concentrating solar power. Applied Thermal Engineering. 2016;109:958-69.
5. Chinnici A, Arjomandi M, Tian Z, Lu Z, Nathan GJ. A novel solar expanding-vortex particle reactor: influence of vortex structure on particle residence times and trajectories. Solar Energy. 2015;122:58-75.
6. Chinnici A, Arjomandi M, Tian Z, Nathan G. A novel solar expanding-vortex particle reactor: experimental and numerical investigation of the iso-thermal flow field and particle deposition. Solar Energy. 2016;133:451-64.
7. Long S, Lau TC, Chinnici A, Nathan GJ. The flow-field within a vortex-based solar cavity receiver with an open aperture. Experimental Thermal and Fluid Science. 2021;123:110314.
8. Davis D, Müller F, Saw WL, Steinfeld A, Nathan GJ. Solar-driven alumina calcination for CO2 mitigation and improved product quality. Green Chemistry. 2017;19(13):2992-3005.
9. Z'Graggen A, Steinfeld A. Hydrogen production by steam-gasification of carbonaceous materials using concentrated solar energy–V. Reactor modeling, optimization, and scale-up. International Journal of Hydrogen Energy. 2008;33(20):5484-92.
10. Cole JA, Parr TP, Widmer NC, Wilson KJ, Schadow KC, Seeker WR. Scaling criteria for the development of an acoustically stabilized dump combustor. Proceedings of the Combustion Institute. 2000;28(1):1297-304.

11. Suksam N, Charoensuk J. Numerical investigation of the effect of constant velocity and constant residence time scaling criteria on the natural gas MILD combustion. Journal of Thermal Science and Technology. 2019;14(2):JTST0022-JTST.
12. Kumar S, Paul P, Mukunda H. Investigations of the scaling criteria for a mild combustion burner. Proceedings of the combustion institute. 2005;30(2):2613-21.
13. Davis D, Jafarian M, Chinnici A, Saw WL, Nathan GJ. Thermal performance of vortex-based solar particle receivers for sensible heating. Solar Energy. 2019;177:163-77.
14. Chinnici A, Davis D, Lau TC, Tian ZF, Saw W, Nathan GJ, editors. First-of-a-kind investigation on performance of a directly-irradiated windowless vortex-based particle receiver. AIP Conference Proceedings; 2020: AIP Publishing LLC.
15. Steinfeld A, Schubnell M. Optimum aperture size and operating temperature of a solar cavity-receiver. Solar Energy. 1993;50(1):19-25.
16. Tian ZF, Nathan GJ, Cao Y. Numerical modelling of flows in a solar–enhanced vortex gasifier: Part 1, comparison of turbulence models. Progress in Computational Fluid Dynamics. 2015;15(2):114-22.
17. Ang D, Chinnici A, Tian Z, Saw W, Nathan GJ. Influence of particle loading, Froude and Stokes number on the global thermal performance of a vortex-based solar particle receiver. Renewable Energy (Submitted).